View metadata, citation and similar papers at core.ac.uk

brought to you by CORE

provided by Elsevier - Publisher Connector

Biochimica et Biophysica Acta 1838 (2014) 2646–2655

Contents lists available at ScienceDirect

Biochimica et Biophysica Acta

journal homepage: www.elsevier.com/locate/bbamem

Cationic liposomes formulated with DMPC and a gemini surfactant traverse the cell membrane without causing a significant bio-damage

E. Stefanutti [a], F. Papacci [b], S. Sennato [a,c], C. Bombelli [d], I. Viola [e], A. Bonincontro [a], F. Bordi [a,c,f], G. Mancini [d], G. Gigli [e,g], G. Risuleo [b,*]

[a] Dipartimento di Fisica, Sapienza Università di Roma, P.le Aldo Moro 2, 00185 Roma, Italy
[b] Dipartimento di Biologia e Biotecnologie, Sapienza Università di Roma, P.le Aldo Moro 5, 00185 Roma, Italy
[c] dCNR-IPCF, Sapienza Università di Roma, P.le Aldo Moro 2, 00185 Roma, Italy
[d] CNR, Istituto di Metodologie Chimiche and Dipartimento di Chimica Sapienza Università di Roma, P.le Aldo Moro 5, 00185 Roma, Italy
[e] National Nanotechnology Laboratory, Institute Nanoscience-CNR (NNL, CNR-NANO), I-73100 Lecce, Italy and c/o Dipartimento di Fisica, Sapienza Università di Roma, P.le Aldo Moro 2, 00185 Roma, Italy
[f] Center for Life Nano Science@Sapienza, Istituto Italiano di Tecnologia, Viale Regina Elena, 291-00161 Roma, Italy
[g] Università del Salento, Dip. di Matematica e Fisica Ennio de Giorgi and Istituto Italiano di Tecnologia, Center for Biomolecular Nanotechnologies, Lecce, Italy

ARTICLE INFO

Article history:
Received 14 February 2014
Received in revised form 14 May 2014
Accepted 24 May 2014
Available online 11 July 2014

Keywords:
Phospholipid liposome
Cationic gemini surfactant
Liposome penetration
Cell surface roughness
Biological effect

ABSTRACT

Cationic liposomes have been intensively studied both in basic and applied research because of their promising potential as non-viral molecular vehicles. This work was aimed to gain more information on the interactions between the plasmamembrane and liposomes formed by a natural phospholipid and a cationic surfactant of the gemini family. The present work was conducted with the synergistic use of diverse experimental approaches: electro-rotation measurements, atomic force microscopy, ζ-potential measurements, laser scanning confocal microscopy and biomolecular/cellular techniques. Electro-rotation measurements pointed out that the interaction of cationic liposomes with the cell membrane alters significantly its dielectric and geometric parameters. This alteration, being accompanied by significant changes of the membrane surface roughness as measured by atomic force microscopy, suggests that the interaction with the liposomes causes locally substantial modifications to the structure and morphology of the cell membrane. However, the results of electrophoretic mobility (ζ-potential) experiments show that upon the interaction the electric charge exposed on the cell surface does not vary significantly, pointing out that the simple adhesion on the cell surface of the cationic liposomes or their fusion with the membrane is to be ruled out. As a matter of fact, confocal microscopy images directly demonstrated the penetration of the liposomes inside the cell and their diffusion within the cytoplasm. Electro-rotation experiments performed in the presence of endocytosis inhibitors suggest that the internalization is mediated by, at least, one specific pathway. Noteworthy, the liposome uptake by the cell does not cause a significant biological damage.

© 2014 Elsevier B.V. All rights reserved.

1. Introduction

Due to their biocompatibility, partial tissue selectivity and relative simplicity of manufacturing, liposomes are among the most studied drug delivery systems (DDS). The validity of liposomes as vehicles for the transport of specific drugs depends on a number of physico-chemical parameters, that are determined by the type and amount of lipids used in their formulation and the physiology of the target system. In the last two decades a particular kind of liposomes, the cationic ones, has raised an increasing interest. Cationic liposomes are formulated with cationic lipids which do not occur naturally and, because of their positive charge, interact more easily with the negatively charged cell membrane and nucleic acids [1]. As a consequence, after the pioneering work of Felgner [2], most investigations have concerned their application as carriers of nucleic acids and, more recently, as vaccine carrier/adjuvants [3,4]. Further, abilities of cationic liposomes to deliver in a fairly specific manner their payload to specific tissues such as tumor endothelium, lungs and liver [5], and gastro-intestinal tract upon oral delivery [6], make them attractive DDS of therapeutic agents for a number of pathologies, among which are the neoplastic ones [7,8]. Due to their ability to increase bacterial cell wall and membrane permeability, thus causing a higher susceptibility to drugs [9,10], cationic liposomes have also been considered as DDS in antibacterial therapies against Gram-negative or antibiotic-resistant bacteria.

As mentioned above, the initial interaction of cationic liposomes with plasma membranes is of electrostatic nature. However, the mode

* Corresponding author at: Dept. Biology and Biotechnology, Sapienza Università di Roma. P. Aldo Moro, 5 - 00185 Rome, Italy.
E-mail address: gianfranco.risuleo@uniroma1.it (G. Risuleo).

http://dx.doi.org/10.1016/j.bbamem.2014.05.026
0005-2736/© 2014 Elsevier B.V. All rights reserved.

of interaction of these, as well as of other nanoparticles, with the cell membrane, the routes of internalization and the intracellular trafficking, yet remain to be fully clarified. On the other hand, the assessment of the internalization pathway, that in turn controls the intracellular traffic and hence determines the target within the cell [11], is a main prerequisite for an optimized drug delivery. As a matter of fact, this information is of the utmost importance to address an adequate design of both new and improved formulations.

The aim of the present study is therefore to analyze the process of the interaction with the cell of a cationic liposome formulation that already demonstrated satisfactory characteristics for pharmacological and gene therapies in terms of delivery and transfection efficiency, stability, and the efficacy of interaction with the cell surface [7,12–15]. To this aim, murine fibroblasts (known as 3T6) in culture were used as a model system.

In particular, the main aim of this work is to discriminate between two possible mechanisms of interaction: the adsorption or adhesion of the liposomes onto the outer surface of the cell membrane, favored by electrostatic interactions and eventually followed by their fusion with the membrane, or their internalization into the cell. This investigation was conducted with the synergistic use of diverse experimental approaches, i.e. electro-rotation (ER) measurements, atomic force microscopy (AFM), ζ-potential measurements, and laser scanning confocal microscopy (LSCM) as well as biomolecular/cellular techniques. ER may reveal membrane alterations measuring the dielectric parameters: specific capacitance, C, and conductance, G, that are related to the membrane structure/functions [16–18]. The surface of cytoplasm membrane of untreated 3T6 cells and of cells of the same line after their exposure to the liposomes was studied using AFM, to gain qualitative and quantitative information about cell surface features [19]. Electrophoretic light scattering technique (ζ-potential measurement) can be informative of the overall charge of the cell surface [20]. LSCM allowed following the pathway of fluorescently labeled liposomes inside the cell [21]. Finally, the biological effects of the liposomes were assessed by means of standard biomolecular/cellular techniques that allow investigating the cell survival/proliferation. By collecting and combining all the results obtained by these different techniques, we were led to conclude that the cationic liposomes under investigation cross the cell membrane, are diffuse within the cytoplasm and do not cause a significant bio-damage.

2. Materials and methods

2.1. Liposome preparation

In all the experiments we used a liposome formulation formed by the zwitterionic phospholipid 1,2-dimyristoyl-*sn*-glycero-3-phosphatidylcholine (DMPC), (Avanti Polar lipids, USA) with the addition of the cationic gemini surfactant (2S,3S)-2,3-dimethoxy-1,4-bis(N-hexadecyl-N,N-dimethylammonium)butane bromide (hereafter Ge1) (Fig. 1), at the molar ratio of 8:2.

The aqueous dispersions of liposomes were prepared by extrusion according to the usual procedure described in the literature [22,23]. Briefly, a film of lipid was prepared by evaporation of a $CHCl_3$ solution containing the appropriate amount of DMPC and Ge1 to obtain the desired molar percentage mixture. One milliliter of PBS buffer solution (Aldrich, 10^{-2} M, pH 7.4) was added to obtain a 12.5 mM lipid dispersion. The solutions were vortex-mixed and freeze-thawed 6× from liquid nitrogen to 307 K. Dispersions were then extruded (10×) at 307 K using a 2.5 mL extruder (Lipex Biomembranes, Vancouver, Canada). The size of liposomes was 110–120 nm, as determined by DLS (cumulant analysis), with a polydispersity index lower than 0.15. The value of ζ-potential was around 26 mV, as obtained from electrophoretic measurements. Liposome suspensions were stable up to 4–5 days.

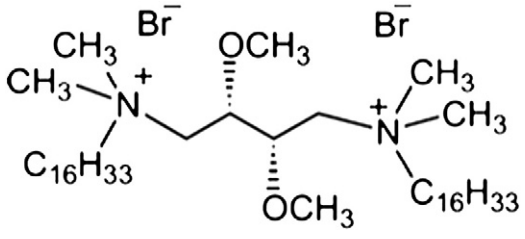

Fig. 1. The synthetic gemini surfactant used for liposome preparation.

Fluorescent liposomes were prepared for the LSCM experiments by adding the fluorescent lipid 1,2-dimyristoyl-*sn*-glycero-3-phosphoethanolamine-N-lissamine rhodamine B sulfonyl ammonium salt (DMPE-RHoB), (Avanti Polar Lipids) to the DMPC–Ge1 mixture in the film preparation (1% of total lipids).

2.2. Cell cultures

The mouse fibroblast cell line 3T6 was used and cells were routinely grown as previously reported [24]. Cultures were exposed to a vast excess of liposomes (in the order of magnitude of 10^6 per cell) for 1 h. These treatment times were selected on the basis of literature data [7,14,15].

In selected electro-rotation experiments bafilomycin A_1 [25] and chlorpromazine [26] were used as endocytosis inhibitors. A bafilomycin A_1 solution was added to the growth medium at 100 nM (f.c.). After 45 min, an aqueous solution of chlorpromazine was added to the growth medium, at 28 μM (f.c.). Total incubation time was 60 min.

The effect of both cationic liposomes and endocytosis inhibitors on cell survival was assessed by the MTT assay (a standard colorimetric assay that measures the reduction of 3-(4,5-diMethyThiazol-2-yl)-2,5-diphenyl tetrazolium bromide, MTT, by mitochondrial succinate dehydrogenase) [27].

2.3. Electrorotation: theory and apparatus

A rotating electric field applied to a poly-dispersed cell suspension induces on each cell a dipole moment, due to the accumulation of charges at the interphase plasma-membrane/solvent [18]. This charge accumulation is a consequence of the high difference in the polarizability between the dispersing medium and the cell membrane. When this mechanism of interfacial polarization relaxes, a phase shift between the electric field and the induced dipole moment occurs. As a consequence, a torque is generated and the cells rotate in an anti-field fashion. The phenomenon is generated in the range of approximately 10^4–10^6 Hz; as the frequency is further increased (≳10 MHz), the electric field traverses the plasma membrane and the direction of cell rotation is inverted in a co-field fashion. In the kHz range, a further relaxation occurs, associated to the double electrical layer formed by the counterions and the mechanisms of surface conductivity. These three relaxations are known as β, γ and α dispersion, respectively. In this study we only considered the β dispersion, directly related to the dielectric properties of the plasma membrane [16,28].

The rotation period (T) of the cell depends on the frequency (f) of the applied field, according to the following equation, which describes a Debye-like relaxation:

$$T(f) = T_{min}\frac{1+\left(\frac{f}{f^*}\right)^2}{2\left(\frac{f}{f^*}\right)} \quad (1)$$

where f^* is the relaxation frequency and T_{min} is the corresponding value of the period. Since the relaxation frequency changes with the conductivity of the dispersing medium σ_e, the measurements were carried out on an osmolar sucrose solution (300 mM) supplemented with NaCl at

the concentrations of: 0, 0.5, 1.0 and 1.5 mM. In these experimental conditions the dependence of f^* upon σ_e becomes linear:

$$f^* = \left(\frac{1}{\pi RC}\right)\sigma_e + \left(\frac{1}{2\pi C}\right)G \quad (2)$$

Following Eq. (2), a linear fit of the relaxation frequency measured at the different solvent conductivities allows to calculate the membrane electric parameters, i.e. the capacitance C and the conductance G per unit surface. Here R is the radius of the cell, assumed to be spherical. An exhaustive overview of the electro-rotation theory can be found in the excellent reviews of Arnold and Zimmermann[29] and of Gimsa [30]. Noteworthy, since in non-living cells the electrical insulation of the membrane is strongly reduced, dead cells do not rotate; as a consequence this technique intrinsically selects metabolically active cells.

An example of data analysis performed on the basis of this model (single-shell, spherical) is reported in Fig. 2 and 3.

We used a standard apparatus for electro-rotation that has been previously described in details [17,24]. The rotating electrical field was generated by superimposing four square waves with a relative phase shift of 90°. These square pulses were applied to the copper mini-plate electrodes of the measuring chamber, which formed a central circular cavity with a volume of about 10 μL. The whole set up was glued onto a microscope slide. The apparatus was connected to a video-recording system that allows a more accurate off-line image analysis. This analysis consists in the measurement of the cell radius and the rotation period at each frequency of the electric field in dispersing media with four different conductivities. A minimum number of 15 cells per frequency value were observed. The conductivities of the four solvents were accurately measured by an impedance meter HP 4194A. The conductance cell is a short section of a cylindrical coaxial line, with stainless steel electrodes, excited far beyond its TM_{01} cutoff frequency, connected by means of an APC-7 connector directly to the input of the meter [31]. The cell is surrounded by a thermostatic jacket that allows to control the sample temperature within ±0.1 °C. Cell constants were determined by measurements with electrolyte solutions of known conductivity using a standard procedure described elsewhere [32]. In the range of electrolyte concentrations considered, the measured conductivity is independent of frequency, from approx 10 MHz down to about 10 kHz within the error. The effect of electrode polarization is

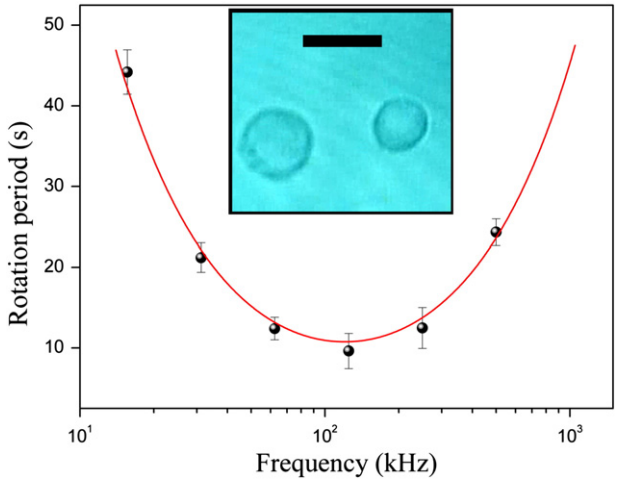

Fig. 2. Typical correlation between cellular rotation period and the frequency of the applied electric field. As an example, the experimental data for sucrose 300 mM (+0 mM NaCl) sample are reported. The curve is the best fit in accordance to Eq. (1). The inset shows two 3T6 fibroblasts with the typical spheroidal appearance that they assume in a suspension when they are not adhering to a substrate, as they appear under the microscope in the electrorotation measuring cell. The bar is 20 μm.

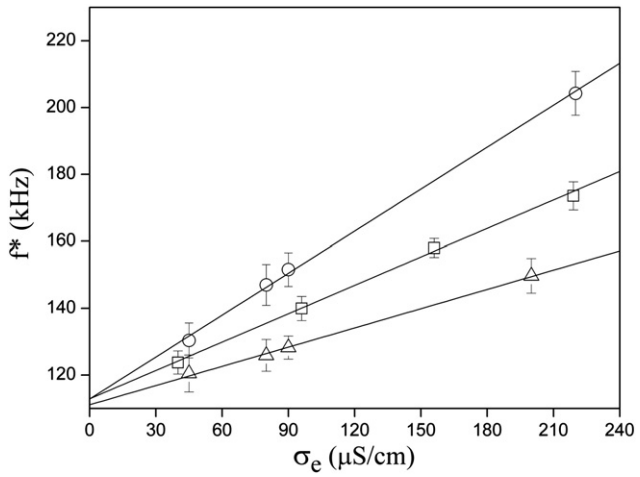

Fig. 3. The relaxation frequency, f^*, as a function of the conductivity of the dispersion medium (σ_e) for: (△) untreated control samples (3T6 cells); (o) 3T6 cells interacting with cationic liposomes DMPC/Ge1 (after 1 h of treatment); (□) 3T6 cells interacting with cationic liposomes DMPC/Ge1 but in the presence of two endocytosis inhibitors (bafilomycin A_1 and chlorpromazine). The straight lines are the best fit of the experimental data obtained according to Eq. (2), using C and G as free parameters to be determined.

significant only at lower frequencies [33]. The overall accuracy, in the range of conductivities investigated is within 1%.

2.4. Atomic force microscopy: image acquisition and sample preparation

AFM measurements were performed in Light Tapping Mode by using a Dimension Icon microscope (Brucker AXS, Germany), simultaneously recording topographic and error images for every analyzed sample. We used high resolution RTESP (Rotated Tapping Etched Silicon) probes, characterized by a sharp tip (radius of curvature specified by the manufacturer R = 8 nm) which is asymmetrically connected to the rectangular cantilever (length 125 mm, nominal resonant frequency 300 kHz, nominal spring constant 40 N/m).

Light Tapping Mode involves maintaining a high amplitude set point relative to the free amplitude of the cantilever. This was chosen as imaging mode because it allows reducing the force applied on a soft sample, thus minimizing membrane alterations and damages due to tip-surface interaction, and avoiding a possible influence of underlying cytoskeleton structures [34–38].

Measurements were performed in air on chemically fixed cells to reveal the topographic modifications caused by the interaction with the liposomes. Noteworthy, also in dry conditions a certain amount of hydration water is retained, allowing reproducible and accurate observations for several hours [35,39]. The acquired images were processed for surface analysis using the Gwyddion 2.28 free software (http://gwyddion.net/). Roughness analysis was performed on all the images. Cells were grown on sterile glass slides in 100 mm-Petri dishes, that were chosen as substrates for AFM measurements. Incubation was continued until the desired cell density was reached, corresponding to no more than one cell for a typical scan size of 50–60 μm. Cells were subjected to chemical fixation with increasing ethanol concentrations employing standard protocols known to minimize alterations of cell morphology [40–42].

2.5. Electrophoretic mobility measurements

Electrophoretic light scattering was used to determine the ζ-potential of cells. This technique offers advantages in terms of accuracy, measurement time and ease of use [20] with respect to other ordinary experimental techniques. A NanoZetaSizer (Malvern Instruments LTD, UK) apparatus equipped with a 5 mW HeNe laser was used. By combining laser Doppler velocimetry (LDV) and phase analysis light scattering

(PALS) [43], this instrument allows the accurate determination of both the average mobility and the mobility distribution. LDV measurements were performed using the so called mixed mode measurement procedure (M3) to reduce electro-osmosis effects [44,45]. The electrophoretic mobility μ was measured and converted into ζ-potential using the Smoluchowski equation [46]$\zeta = \mu\eta/\epsilon$, where η and ϵ are the viscosity and the permittivity of the solvent phase, respectively. This equation is generally valid for large particles, with a ratio of the particle radius to the Debye length larger than five [47]. Measurements were performed at 25 °C by suspending the 3T6 cells incubated with liposomes in a solution of sucrose 300 mM. Dilution ratios (N_L/N_C: number of liposomes/number of cells) were obtained ranging between 1 and 10^7.

2.6. Laser scanning confocal microscopy (LSCM): images acquisition and sample preparation

LSCM experiments were performed on an Olympus FV1000 confocal microscope. A multiline Argon laser ($\lambda = 515$ nm) was used as the excitation source, equipped with a excitation dichroic mirror DM458/515 and a 60×/1.40 NA oil-immersion objective. The microscope was operated setting the pinhole aperture at 70–80 μm, thus resulting in a 200 nm for the XY-resolution and about 400 nm for the axial resolution (along Z axis). All the images were obtained with a resolution of 1024 px × 1024 px. The laser excitation induced the emission of fluorescence by rhodamine-labeled phospholipids embedded in the double layer of the liposome membrane (see Section 2.1). Every cell was observed at room temperature (20–25 °C) for a time interval in the order of 1–3 h. The 3D confocal scanning was performed by a Z-stack sequential acquisition. Optical sections were collected in transverse XZ and YZ planes. Spatially-resolved fluorescence spectra (SR-F) were collected with a wavelength resolution of 2 nm.

Specific glass bottom-dishes (WillCo-dish Glass Bottom, Willco Wells, 40 mm in diameter and 0.17 mm in thickness) were used as substrate. Cells were subsequently exposed to an excess of rhodamine-labeled liposomes at the same liposome–cell ratio chosen for the other experiments ($N_L/N_C \approx 10^6$). Treatment time with liposomes was 1 h. Cells were not subjected to fixation and trypsinization before being observed. Moreover samples were thoroughly washed several times with fresh DMEM [48,49].

3. Results and discussion

3.1. Electrorotation

The results of the electro-rotation measurements carried out on 3T6 cells exposed for 1 h to DMPC/Ge1 liposomes further validate previous observations from our laboratory [15]. The interaction with the DMPC/Ge1 causes a significant variation of the dielectric parameters of the plasma membrane, as pointed out in Fig. 3.

In particular, a drastic reduction of both the specific capacitance C and conductance G (in the order of 60%) is observed. This reduction is associated to a variation of the average cell radius, which increases to about 10% (Table 1). Changes of the dielectric parameters, that in this case apparently did not affect the cell viability, as shown by the MTT data as discussed in details below, are in general the result of different concomitant causes, reflecting changes in the membrane organization (ϵ_m') and ionic permeability (σ_m), and in the membrane thickness. It is worth to note that in this context, the "membrane thickness" must be interpreted as an average or "effective" thickness of the "membrane domain" [50,18], which takes into account the membrane roughness and sinuosity [51]. Strictly speaking, a change of the bilayer thickness could imply a partial mismatch of the membrane protein moiety with the lipid matrix [52], and a consequent impairment of the protein function. However, the fact that the observed changes do not interfere significantly with the cell functionality, suggests that they have to be ascribed mainly to a variation of the membrane effective thickness or, in other words, to changes of the membrane roughness and sinuosity. The marked effect that membrane microvillosity can have on the membrane dielectric parameter measured in dielectric spectroscopy experiment has been pointed out by various authors ([53,54] and the literature cited therein) and also recently by Asami [55].

In fact, the simple description of a cell which is generally adopted in the literature to model its dielectric properties [56,16,51] is that of a sphere surrounded by a thin homogeneous layer, which mimics the plasma membrane with its roughness. In this picture, the cell is assimilated from the electrostatic point of view to a spherical capacitor. Clearly, the intrinsic surface roughness of the membrane increases its effective area, thus making the cell rather different from an ideal smooth sphere. For this reason, a dimensionless form factor ($\phi_m \geq 1$) is usually introduced to account for the difference between the geometrical and the effective surface. The expression for the specific capacitance thus becomes $C = \phi_m \epsilon_0 \epsilon_m / d$ (with ϵ_0 the vacuum permittivity). Clearly, this schematization affects also the specific conductance, which becomes $G = \phi_m \sigma_m / d$. For different cell lines such form factor ϕ_m was experimentally evaluated to be between 1.5 and 2.0 [57,58]. In these terms, the observed reduction of the membrane dielectric parameters as a consequence of the exposure to the liposomes can be interpreted as reflecting a decrease of ϕ_m, or in other words an overall smoothing of the cell surface. Such smoothing and flattening of the membrane roughness are qualitatively consistent with the observed increase of the cell radius.

In Table 1 and Fig. 3 are presented also the results of ER experiments conducted in the presence of specific endocytosis inhibitors.

Interestingly, upon incubation with cetyltrimethylammonium bromide (CTAB), at increasing concentrations, c_s, of this cationic surfactant but below its critical micellar concentration, CMC, ($CMC_{CTAB} = 1mM$ at T = 25 °C) yeast cells exhibit at first an increased membrane capacitance, C_m. Then, having reached a maximum at $c_s \approx 0.3$ the capacitance C_m decreases. Such changes of C_m are accompanied by a marked (and monotonous) decrease of the cell radius (shrinkage) [54]. Also in that case the observed variation of C_m was interpreted as due to changes in the membrane folding. In fact, the initial increase of C_m was attributed to an augmented folding of the membrane, while the subsequent decrease was interpreted in terms of a solubilization of the "excess folds" of the membrane, resulting in practice in a flattening, favored by the relatively high concentration of the surfactant [54]. It must be noted that in that study the surfactant molecules, being dissolved in the suspending medium at low concentration, interacted with the cell membrane as single molecules. On the contrary, in the present study the interaction is between the cell and the liposomes that, although built up with cationic lipids, nevertheless interact with the cell as single nanoscopic structures. The chemical structure of Ge1, the cationic surfactant employed here, has some resemblance with the CTAB. In fact, Ge1 can be imagined made of two CTAB molecules whose polar heads are linked together by a short "spacer" chain three carbon atoms long. However, its properties as a surfactant, and in particular its packing parameter [52] and hence its ability of forming structures [59], are rather different from that of the single tail CTAB. Nevertheless, some comparison between the behavior of the structure as a whole, the liposome, and the component molecules can be made.

Table 1
Percent variation of the specific dielectric membrane parameters (C and G) and the average cell radius (R) for cell samples obtained with three different treatments: interaction with DMPC/Ge1 for 1 h, interaction with molecules that behave as endocytosis inhibitors for 1 h, interaction with DMPC/Ge1 in presence of endocytosis inhibitors for 1 h.

	$\Delta C/C$(%)	$\Delta G/G$(%)	$\Delta R/R$(%)
DMPC/Ge1	−60±4	−64±2	13±3
Endocytosis inhibitors[a]	2±5	5±4	0.1±4.6
Endocytosis inhibitors[a] + DMPC/Ge1	−38±8	−44±7	6±2

[a] Bafilomycin A_1 and chlorpromazine.

It is worth noting that this could be a typical example of the situation that usually occurs in bio-nano-technologies: once a nanostructure is built up, the mechanisms of its interaction with complex biological structures can be completely different from those of the component molecules with the same structures.

3.2. AFM

To investigate in more detail the changes of membrane morphology we employed Tapping Mode AFM. Fig. 4 shows typical AFM images of single 3T6 cells, untreated (upper row) and after incubation with DMPC/Ge1 (lower row). The cells show the typical shape of 3T6 fibroblasts adhering to a hydrophilic substrate (see for example [60]), a clear indication that the fibroblasts are and remain well anchored to the substrate during the AFM scanning operations.

In Fig. 4A and E different regions can be easily identified: a prominent nuclear area is clearly visible, surrounded by a flatter surface corresponding to the cytoplasm. Such a marked heterogeneity has been observed also for other cell lines [61,62]. As expected, due to ethanol fixation the cells show a marked dehydration, that yields a significant reduction of cell volume. However, the dehydration process does not dramatically alter the cell morphology: the nuclei are clearly visible and never collapsed and in several frames indications of the presence of nucleoli can be also found. In addition, cytoplasmic areas keep their usual smooth appearance, although traces of well-recognized artifacts (e.g. volcano-like depressions) occur locally [40,42]. When present, the areas affected by such artifacts were not considered in the quantitative analysis of surface roughness.

An additional evidence of the fact that the fixation and the imaging technique are able to preserve satisfactorily the morphology of the cell surface comes from the observation of several membranous and submembranous structural details. Such details, that have been described also by other authors, can be more easily recognized in the images obtained in the "error signal mode" (Fig. 4B and F) that provides images related to the first derivative in scan direction of the topography, hence emphasizing edges and details of the surface [63]. In these images the following details can be observed: rigid filamentous structures probably belonging to the cytoskeletal network [64] (Fig. 4B, white arrows) or identifiable as microtubules (Fig. 4B and F, blue arrow, and the red circle in panel H); small round bodies of micrometric size, that can be interpreted to be single spots of myosin [65] or vesicles [66] (Fig. 4B, black arrows); actin filaments running underneath the cell membrane, especially localized at the periphery of the cell (Fig. 4C, white arrows) [41,67,68,60] and usually forming stress fibers [37,66] and a typical cell junction (Fig. 4C, white circle).

After incubation with liposomes, the qualitative appearance of the cell surface morphology does not change. Actin filaments (Fig. 4F, white and black arrows and Fig. 4G, black arrows) and stress fibers (Fig. 4F, black circle) are still observed. Protruding membrane structures that correspond to microprocesses such as filopodia (Fig. 4F, black square and Fig. 4G, white arrows) and lamellipodia (Fig. 4F, black arrow) can also be identified. In some cases, small protruding structures, presumably ruffles (Fig. 4F, blue arrow), are shown upon the top of lamellipodia.

However, a significant alteration in the cell height, in fact an average increase of ≈200 nm, is observed. In the examples shown, the height increases from about 800 nm to more than 1 μm (compare the profiles shown in Fig. 4D and H).

In order to obtain a more quantitative comparison of the membrane surface details between treated and untreated samples, we analyzed the statistical properties of the surface roughness. The roughness of the plasma membrane, being involved in several cellular mechanisms such as adhesion and motility, is an important cytological parameter and is considered a sensitive indicator of alterations of cell metabolism. For example, the roughness measured in AFM images of whole cells or of cell subregionshas been used to evidence the effect of drugs, mechanical stress or of the aging, on different cell lines [69–71].

In most AFM studies the cell membrane surface roughness is characterized in terms of the root-mean-square roughness parameter R_{RMS}, i.e. the standard deviation of the distribution of the z-values within the scanned area [71,72]. However, this parameter is in general "scale dependent", i.e. it increases with the scanning area [73,70,72], and such dependence makes it difficult to compare different images and/or different areas of the images. Moreover, a description of the morphology of surfaces in terms of root-mean-square roughness on a given scale length is often unsatisfactory since, for example, surfaces with rather different morphology, and hence different properties of adhesion, may show the same values of R_{RMS}[74,75]. Conversely, surfaces characterized by different values of R_{RMS} may show similar adhesive or tribological behaviors.

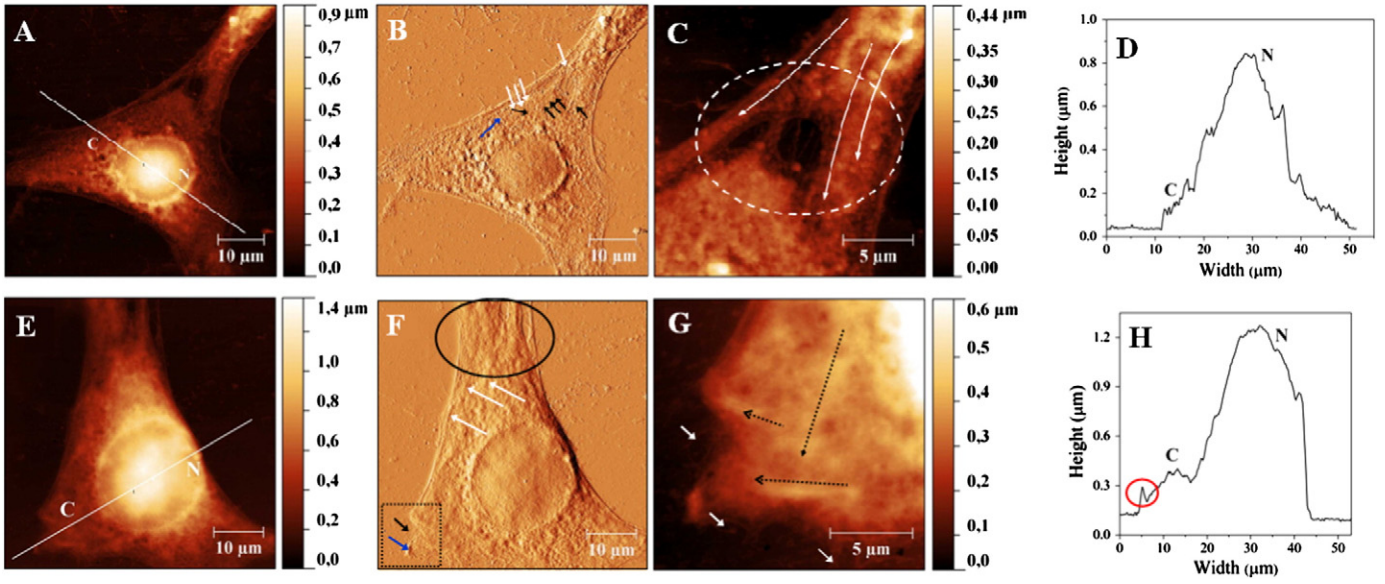

Fig. 4. Tapping Mode AFM images of 3T6 cells untreated (upper row) and after (lower row) liposome incubation. Height (A, E) and amplitude error (B, F) images (scan size 55 × 55 μm^2) of single 3T6 cells, showing well distinct nuclear (*N*) and cytoplasmic (*C*) regions. Panels C and G are details of the same images (A and E) but at higher magnification. Panels D and H show the height profiles along the white lines in panels A and E, respectively. Arrows and circles in panels B, C, F and G mark different morphological details such as actin filaments and microtubules, see text for a detailed explanation.

The surface roughness can be more effectively characterized by calculating instead the power spectral density (PSD) defined as [74]

$$\mathrm{PSD}(\mathbf{q}) = \frac{1}{(2\pi)^2}\int d^2x <h(\mathbf{x})h(0)> e^{-\mathbf{q}\cdot\mathbf{x}} \tag{3}$$

where $\mathbf{x} = (x, y)$, and $z = h(x)$ is the surface height measured from the average surface plane, i.e. the plane where $< h > = 0$. The $< \ldots >$ indicates ensemble averaging, i.e., averaging over a collection of different surfaces (or different portions of the surface) with identical statistical properties. In fact, the PSD is the Fourier transform of the height autocorrelation function.

In AFM experiments, where the surface is scanned along parallel lines, it is usual to evaluate the one-dimensional power spectral density function, based only on profiles along the fast scanning axis [74]

$$\mathrm{PSD}_1(q_x) = \int \mathrm{PSD}\left(q_x, q_y\right) dq_y \tag{4}$$

This function can be evaluated from the discrete AFM data values, using the Fast Fourier Transform algorithm, as [76]

$$W_1(K_x) = \frac{h}{2\pi NM}\sum_{j=0}^{N}\left|\sum_{k=0}^{N} z_{kj} exp[-i\ K_x\ k\ h]\right|^2 \tag{5}$$

where N and M are the number of rows and columns of the data field, respectively, and h is the distance between the experimental points along the scanning line.

As an example, Fig. 5 shows the quantity W_1 as a function of the spatial wavenumbers K_x calculated for the two typical images of 3T6, one treated with liposomes and the other untreated, shown in Fig. 4.

Notably, in the lowest range of spatial frequencies, the PSD of the treated cell is almost one order of magnitude larger than that of the untreated one. Conversely, in the high frequency range the PSD of the untreated one is larger by a factor of 2. Such differences appear systematically when the images of treated and untreated cells are compared in terms of PSD, and find a simple interpretation in terms of cell swelling upon the incubation with the liposomes. In fact, while the swelling increases the size of the cell as a whole (and hence all the features whose size is on the whole-cell scale), the resulting stretching of the membrane has the effect of smoothing out the small scale roughness on the membrane surface. Such interpretation is perfectly consistent with the observed increase of cell volume, and with the smoothening of the cell surface hypothesized in the previous section to justify the changes of the dielectric membrane parameters measured by ER.

The different "quality" of the membrane roughness for treated and untreated cells may be characterized in a more quantitative manner by noting that over several frequency decades both the PSD curves in Fig. 5 show a well defined linear behavior in the log–log scale. This means that in this interval the surfaces are self-affine fractals that can be characterized by a well defined fractal dimension.

A self-affine fractal surface has the property that if the surface is magnified, then the new surface "still looks the same". In other words the statistical properties of the surface are invariant under the scale transformation.

For a self-affine surface the power spectrum has the power-law behavior [74]

$$\mathrm{PSD}(\mathbf{q}) \sim q^{-2(H+1)} \tag{6}$$

where the Hurst exponent H is related to the surface fractal dimension D_f through the relationship [77] $H = 3 - D_f$. It is easy to see that for the unidimensional power spectral density Eq. (4), and hence for the discrete $W_1(K_x)$, the correct exponent is $W_1(K_x) \sim q^{-2(H\ +\ 1)\ +\ 1}$. On a log–log scale a power law becomes a straight line, with a slope equal to the power law exponent. The fractal dimension of the surface can be hence easily calculated from the slope β of a linear fit on log–log scale in the frequency interval where the curves are approximately linear, the fractal dimension being $D_f = (7 - |\beta|)/2$.

By using the dedicated procedure of the Gwyddion software we calculated the fractal dimension D_f for all the images acquired, both treated with liposomes and untreated. Consistently with the hypothesis of a swelling of the treated cells and a consequent stretching of their membrane, we obtained for the fractal dimension of the untreated cells an average value of 2.17 ± 0.07, and for the D_f of the treated ones the smaller value, indicative of a smoother surface, of 2.03 ± 0.05.

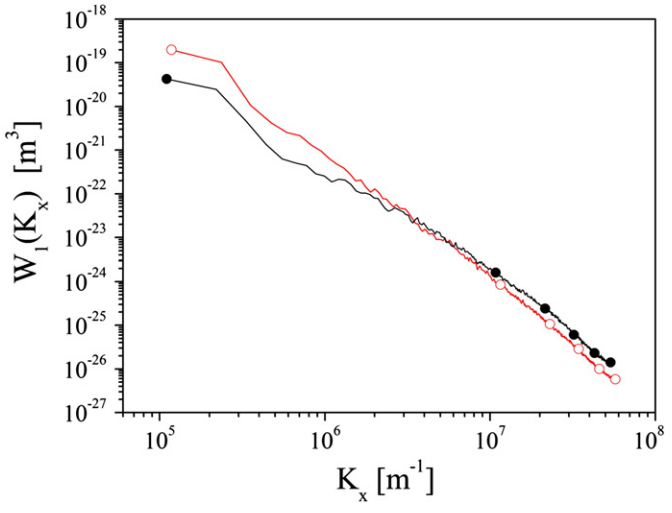

Fig. 5. In this example the power spectral density W_1 is calculated as a function of the spatial wavenumbers K_x for the two typical images of 3T6, one untreated (full symbols) and the other treated with liposomes (empty symbols), shown in Fig. 4 panels A and E. In the lowest range of spatial frequencies, the PSD of the treated cell is larger than that of the untreated one, while in the high frequency range it is exactly the opposite. Moreover, in a wide frequency interval, that extends over several decades, both the PSD curves show in the log–log scale a well defined linear behavior: in this interval the surfaces are self-affine fractals characterized by defined fractal dimensions (see text).

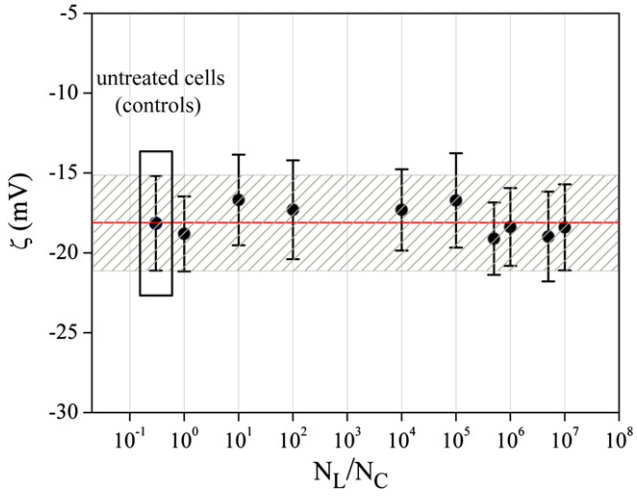

Fig. 6. ζ-potential of 3T6 cells after incubation with liposomes, as a function of the N_L/N_C ratio. ζ-potential value of 3T6 cells without liposomes is shown as reference (highlighted by the black box), with the relative error band (lined region). Error bar associated to each point has been obtained as the standard deviation of the measurements performed at the same dilution ratio, while the red line corresponds to the average of all the measurements obtained for every N_L/N_C.

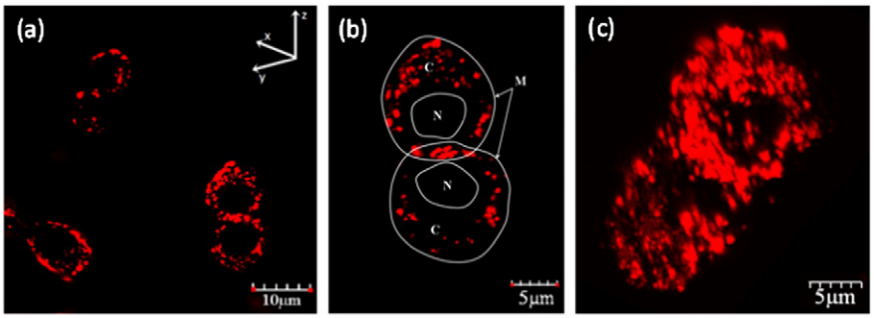

Fig. 7. (a) Z-stack confocal images of the specimen. Liposomes (or their aggregates) are labeled with rhodamine (red spots). The time interval between the incorporation of stained liposomes in the cell medium and the observation under confocal microscopy was 1 h. (b) Single XY slice image showing a particular of panel (a) with two partially overlapping cells. The contours of the cells (M) and of the cell nuclei (N), as they appear in Brightfield images of the same field superimposed to the fluorescence images, are outlined in white. A large amount of liposomes are recognizable in the cytoplasmic area (C). (c) 3D visualization of the two cells in panel (b). The images have been obtained by digital reconstruction of a Z-stackconfocal scanning with a 450 nm resolution along the optical Z axis.

A final comment on the observed dependence of the root mean square roughness on the scan size L is in order. It is easy to see [74] that

$$R_{RMS}^2 = \langle h^2 \rangle = \int d^2x \, \mathrm{PSD}(\mathbf{q}) \tag{7}$$

Clearly, in experiments the integration is limited in practice by the lateral size L of the scanned area (or of the sample surface). For a self-affine fractal surface, where the PSD decreases with a power law, the integral (Eq. 7) is mainly determined by the fluctuations of the surface height with the maximum possible wavelength λ_{max}. Then, since for a given scanning size L and for a self affine surface the condition $\lambda_{max} \sim L$ holds, the value of the integral will depend on the size L of the scanned area. In other words, the dependence on L of the calculated value of R_{RMS} is simply a consequence of the fact that $L \sim \lambda_{max}$ and not $L \gg \lambda_{max}$, and in this case averaging over the whole surface area is not identical to ensemble averaging. To obtain an L-independent roughness a scan size $L \gg$ of the typical cell size should be chosen, so to include several cells in the image and have $L \gg \lambda_{max}$, but in this way the details of the roughness at the smaller scale should probably be lost. For this reason a characterization of the roughness surface in terms of PSD function instead of R_{RMS} seems to be preferable [74,75].

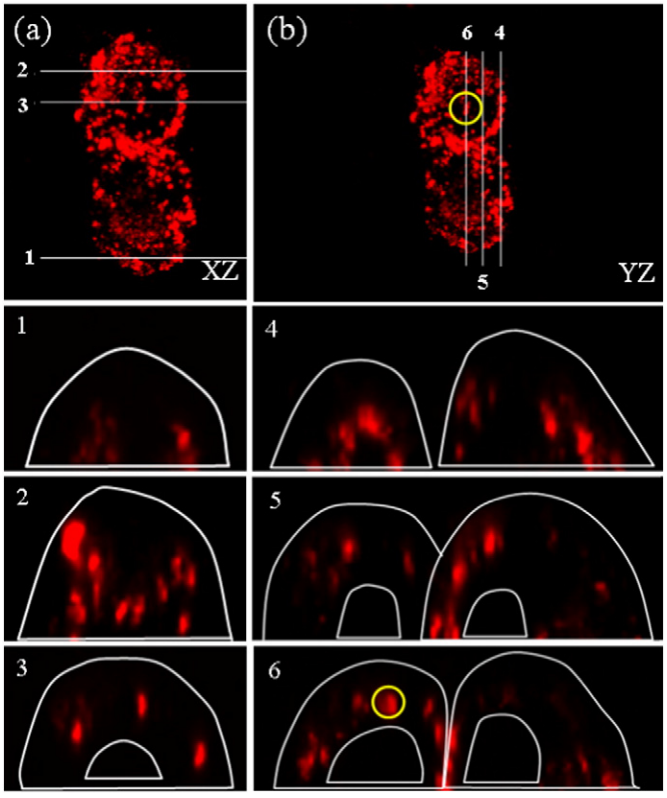

Fig. 8. The left (right) side of the image shows liposome distribution within XZ (YZ) slices obtained sectioning the sample as indicated in panel (a) ((b)), that depicts the projection superimposition of the XY-slices perpendicular to the Z-optical axis (1 h interaction). White lines represent in a simplified manner the cell plasma membrane and the nuclear membrane outlines. They have been traced using the same procedure as in Fig. 7 and serve as an indication, in order to make the identification of the main cellular spaces easier. The yellow circle marks a liposome cluster that could appear located within the nucleus (panel (b)), however section number 6 clearly shows that the cluster is in the cytoplasm and above the nucleus.

3.3. Electrophoretic light scattering measurements

To address whether the interaction cell/liposome affects the surface charge of the membrane, we evaluated the ζ-potential of cells after incubation with liposomes at different dilution ratios N_L/N_C. We considered a DMPG–Ge1 liposome as a sphere of 110–120 nm in diameter, as determined by DLS measurements [59], and the area occupied by a single lipid molecule at the liposome surface ≈ 70 Å^2. Neglecting, as a first approximation, the differences between the two components and the packing effects connected to the steric or electrostatic interaction between the two lipids in the mixture, we estimated the aggregation number and hence the number of liposomes in the suspension. By keeping constant the number of cells in each sample ($\approx 10^6$ cells), starting from a condition of large excess of liposomes, we explored a broad range of N_L/N_C, down to the limit condition of 1 liposome per cell.

In the absence of liposomes, the 3T6 cells suspended in sucrose 300 mM showed a negative ζ-potential (-18 ± 3 mV) confirming that, as expected, at physiological pH and ion strength their surface charge is weakly negative [78].

Notably, also after 1 h of incubation with different concentrations of DMPC–Ge1 liposomes the ζ-potential of the cells did not show any significant variation.

In fact, Fig. 6 shows that the ζ-potential of the cells remains close to the negative value exhibited by the untreated cells at all the N_L/N_C ratios, indicating that the charge density on the outer cell surface is not significantly affected by the interaction with the positively charged liposomes. This result rules out the adsorption of the liposomes on the outer cell membrane. It also seems to exclude a process of fusion followed by the accumulation of the positively charged lipids into the cell membrane. It rather suggests that the liposomes simply traverse the membrane to be internalized into the cytoplasm.

This is consistent with the observation that after the interaction with the liposomes, the cells remain vital (see Section 3.5).

The results obtained from ER measurements conducted in the presence of the endocytosis inhibitors [79] bafilomycin A_1 (a specific

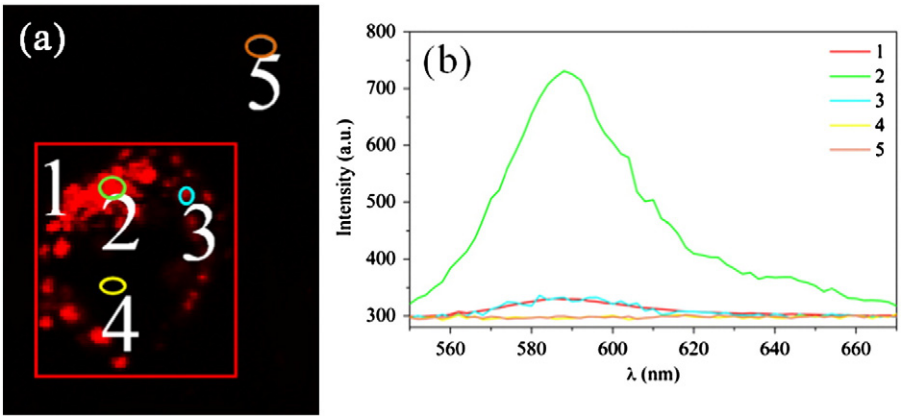

Fig. 9. (a) Confocal microscopy image of a cell interacting with stained liposomes. (b) Spatially resolved fluorescence spectra of the same area captured in image (a), recorded for different regions of interest (ROI): a single cell (red rectangle, ROI 1); a region that exhibits a high density of liposomes (green circle, ROI 2); a single spot (cyan circle, ROI 3) that should represent a single liposome or a little aggregate; nuclear inner region (yellow circle, ROI 4) and the background, namely the glass slide used as substrate (orange circle, ROI 5). By exciting the specimen with a $\lambda_{ex} = 515$ nm radiation, a noticeable emission peak occurs at $\lambda_{em} = 588$ nm, in correspondence to the high-density-rhodamine region. An almost null intensity is recorded for ROI 4 suggesting that liposomes do not diffuse into the nucleus after 1 h. ROI 5 is taken as a control.

inhibitor of the vacuolar proton pump) [80] and chlorpromazine (a drug that disrupts clathrin-dependent endocytosis) [81] give further evidence that the observed alterations of the dielectric parameters are connected with the passage of the liposomes through the membrane and not with their incorporation into the bilayer. In fact, in the presence of the inhibitors the effect on the dielectric parameters is drastically reduced (Table 1, bottom line, and Fig. 3). Note that, in the absence of the liposomes, the presence of the inhibitors does not cause any significant change in the dielectric and geometric parameters of the cell membrane (Table 1, middle line).

3.4. Laser scanning confocal microscopy

The liposome location within the cell was addressed by Z-stack acquisitions, to have a digital 3D reconstruction of the specimen (Fig. 7) and to get XZ and YZ sections (see Fig. 8) [49]. The LSCM images show several liposomes, detected mainly in the cytoplasmic area (Fig. 7 and 8).

By inspecting all the images and the spatial resolved fluorescence (SR-F) spectra (Fig. 9), the presence of well defined red spots emitting in the expected wavelength range ($\lambda_{em} = 588$ nm) revealed that the liposomes remain stable and intact at least after 1 h of treatment. As a matter of fact if they had been damaged during or after the internalization, a homogeneous fluorescence would have been observed spreading over the cytoplasm.

Note that the isotropy of fluorescence emission somehow masks the actual dimensions of the light source (emitter). Therefore, the spot size in the images is not the actual size of the liposomes, which, in addition, is close to the microscope resolution power ($R_{XY} = 200$ nm and $R_z = 400$ nm, as reported in Section 2.6).

The confocal optical sections shown in Fig. 8 clearly point out that the liposomes do not remain adsorbed on the cell membrane, but that they are internalized into the cytoplasm. In Fig. 8, section number 1 (panel a) and number 4 (panel b) were taken close to the cell edge, where the fluorophore density is quite low. In section No. 2 a comparatively larger density of the fluorophore appears. Section Nos. 3, 5 and 6 cut across the cell nucleus. Liposomes are localized around its outer limit, but they are never detected within the nucleoplasm. A further evidence supporting the absence of liposomes within the cell nucleus is provided by the yellow circle around section No. 6: in the XY projection (panel b) red spots do appear in the nuclear area, but section No. 6 clearly shows that they are actually located within the cytoplasm, being simply above to the nucleus (and hence superimposed to it in the XY projection).

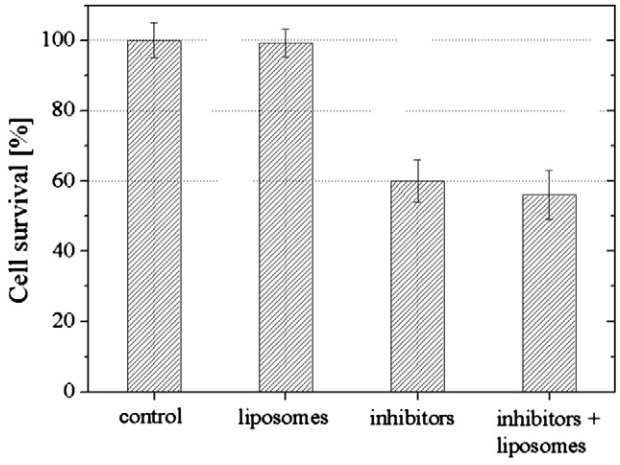

Fig. 10. MTT assay performed on: (from left to right) 3T6 control cells; the cells after the interaction with the liposomes (1 h); the cells in the presence of the sole endocytosis inhibitors; the cells after the interaction with the liposomes in the presence of the inhibitors.

3.5. MTT assay

Fig. 10 shows the results of the MTT assay performed on 3T6 cells interacting with the cationic liposomes DMPC/Ge1. Apparently, the cell vitality is not affected by the interaction with the liposomes, as already reported in [15]. The endocytosis inhibitors show an important toxicity, causing a 40% decrease in cell viability. The exposure to DMPC/Ge1 does not significantly alter the number of alive cells. This result clearly validates the idea that DMPC/Ge1 does not cause a significant bio-damage to 3T6 cells.

4. Final considerations and conclusions

The combined results provided by AFM and ER measurements demonstrate that the cell roughness decreases as a consequence of the liposome/cell interaction. Such smoothening of the surface, and the concomitant increase of the average radius of the cells suggest that upon interaction the cells swell significantly. It is known, as a matter of fact, that mammalian cells can easily accommodate moderate volume increases (< 2-fold) by stretching their surface and drawing lipid bilayer material from preexisting reserves [82]. For example, Grygorczyk and co-workers have shown that during a twofold membrane reduction in extracellular tonicity, all increase in surface area could essentially be

attributed to unfolding of the plasma membrane, whereas more dramatic cell swelling was associated with endomembrane insertion[83].

By hypothesizing, for the sake of simplicity, that the cell swelling and the consequent smoothening of the membrane surface are due solely to the volume increase (ΔV_C) caused by the liposome entry into the cytoplasm, considering that the average radius of our liposomes is ≈60 nm (from dynamic light scattering measurements [84]), the average radius of untreated control cells was $R_C = 8.5 \pm 0.3$ μm and that the observed increase of R_C after 1 h of treatment is $\Delta R_C/R_C = 0.13$ (see Table 1), one can calculate the order of magnitude of the number of liposomes within the cell, n, simply as

$$n = \frac{\Delta V_C}{V_C}\left(\frac{V_C}{V_L}\right) = 3\frac{\Delta R_C}{R_C}\left(\frac{R_C}{R_L}\right)^3 \quad (8)$$

This results in a very high number of entrapped liposomes per cell, of the order of 10^6, which is comparable to the total number of particles per cell employed in the treatment: in practice, all the available liposomes would be captured by the cells.

While this is a very rough estimation, this result seems to point out a very high uptake efficiency, which makes these liposomes very attractive vectors for different bio-nano-technological strategies. The results obtained by ER and AFM evidence a significant effect on the plasma membrane but do not give information on the actual interaction mechanisms. To address this point we carried out measurements of ζ-potential on liposome-treated cells at different ratios DMPC/Ge1-cell, varying in this way the probability of interaction. The ζ-potential remains unvaried both in the control and in the liposome-treated cells. Since ζ-potential is directly proportional to the surface charge density (in the same condition of pH, ion strength and geometry of cells), its stability clearly demonstrates that the charge exposed on the cell outer surface does not vary in a significant manner. Such a result rules out the hypothesis of a static adsorption on the cell surface mediated by electrostatic forces, or that of a fusion of the liposomes with the membrane. ER experiments, conducted in the presence of specific inhibitors of endocytotic processes (bafilomycin and chlorpromazine) reveal a direct involvement of (at least one) endocytotic pathway in the interaction mechanism. In fact, the significant reduction of the effect on the dielectric parameters C and G as well as on the radius R, observed in these experiments points out the significant decrease in the liposomes uptake due to the endocytosis inhibitors. Finally, LSCM experiments clearly show that the liposomes traverse the plasma membranes and remain located within the cytoplasm. Furthermore, the phenomenon occurs without any significant biological damage.

Acknowledgments

SS and CB acknowledge funding under the MIUR Basic Research Investigation Fund (FIRB/2012) program Grant No. RBFR12BUMH.

References

[1] D. Simberg, S. Weisman, Y. Talmon, Y. Barenholz, DOTAP (and other cationic lipids): chemistry, biophysics, and transfection, Crit. Rev. Ther. Drug Carrier Syst. 21 (2004) 257–317.
[2] P.L. Felgner, T.R. Gadek, M. Holm, R. Roman, H.W. Chan, M. Wenz, J.P. Northrop, G.M. Ringold, M. Danielsen, Lipofection: a highly efficient, lipid-mediated DNA-transfection procedure, Biochemistry 84 (1987) 7413–7417.
[3] A. Joseph, N. Itskovitz-Copper, S. Samira, O. Flasterstein, H. Eliyahu, D. Simberg, I. Goldwaser, Y. Barenholz, E. Kedar, A new intranasal influenza vaccine based on a novel polycationic lipid-ceramide carbamoyl-spermine (CCS) I. Immunogenicity and efficacy studies in mice, Vaccine 24 (2006) 3990–4006.
[4] C. Lonez, M. Vandenbranden, J.M. Ruysschaert, Cationic liposomal lipids: from gene carriers to cell signalling, Prog. Lipid Res. 47 (2008) 340–347.
[5] C. Dass, P.F.M. Choong, Targeting of small molecule anticancer drugs to the tumour and its vasculature using cationic liposomes: lessons from gene therapy, Cancer Cell Int. 6 (2006), http://dx.doi.org/10.1186/1475-2867-6-17.
[6] T. Jubeh, Y. Barenholz, A. Rubinstein, Differential adhesion of normal and inflamed rat colonic mucosa by charged liposomes, Pharm. Res. 21 (2004) 447–453.
[7] C. Bombelli, G. Caracciolo, P.D. Profio, M. Diociaiuti, P. Luciani, G. Mancini, C. Mazzuca, M. Marra, A. Molinari, D. Monti, L. Toccacieli, M. Venanzi, Inclusion of a photosensitizer in liposomes formed by dmpc/gemini surfactant: correlation between physicochemical and biological features of the complexes, J. Med. Chem. 48 (2005) 4882–4891.
[8] A. Molinari, C. Bombelli, S. Mannino, A. Stringaro, L. Toccacieli, A. Calcabrini, M. Colone, A. Mangiola, G. Maira, P. Luciani, G. Mancini, G. Arancia, m-THPC-mediated photodynamic therapy of malignant gliomas: assessment of a new transfection strategy, Int. J. Cancer 121 (2007) 1149–1155.
[9] M.R. Hamblin, T. Hasan, Photodynamic therapy: a new antimicrobial approach to infectious disease? Photobiol. Sci. 3 (2004) 436–450.
[10] C. Bombelli, F. Bordi, S. Ferro, L. Giansanti, G. Jori, G. Mancini, C. Mazzuca, D. Monti, F. Ricchelli, S. Sennato, M. Venanzi, New cationic liposomes as vehicles of m-tetrahydroxyphenylchlorin in photodynamic therapy of infectious diseases, Mol. Pharm. 5 (2008) 672–679.
[11] L. Rajendran, H.-J. Knölker, K. Simons, Subcellular targeting strategies for drug design and delivery, Nat. Rev. 9 (2010) 29–42.
[12] A. Molinari, M. Colone, A. Calabrini, A. Stringaro, L. Toccacieli, G. Arancia, S. Mannino, A. Mangiola, G. Maira, C. Bombelli, G. Mancini, Cationic liposomes, loaded with m-THPC, in photodynamic therapy for malignant glioma, Toxicol. in Vitro 21 (2007) 230–234.
[13] C. Bombelli, F. Faggioli, P. Luciani, G. Mancini, M.G. Sacco, Efficient transfection of DNA by liposomes formulated with cationic gemini amphiphiles, J. Med. Chem. 48 (2005) 5378–5382.
[14] C. Bombelli, A. Stringaro, S. Borocci, G. Bozzuto, M. Colone, L. Giansanti, R. Sgambato, L. Toccaceli, G. Mancini, A. Molinari, Efficiency of liposomes in the delivery of a photosensitizer controlled by the stereochemistry of a gemini surfactant component, Mol. Pharm. 7 (2009) 130–137.
[15] R. Cosimati, G. Milardi, C. Bombelli, A. Bonincontro, F. Bordi, G. Mancini, G. Risuleo, Interactions of DMPC and DMPC/gemini liposomes with the cell membrane investigated by electrorotation, Biochim. Biophys. Acta 1828 (2013) 352–356.
[16] K.R. Foster, F.A. Sauer, H.P. Schwan, Electrorotation and levitation of cells and colloidal particles, Biophys. J. 63 (1992) 180–190.
[17] A. Bonincontro, V.D. Ilio, O. Pedata, G. Risuleo, Dielectric properties of the plasma membrane of cultured murine fibroblasts treated with a nonterpenoid extract of *Azadirachta indica* seeds, J. Membr. Biol. 215 (2007) 75–79.
[18] H. Morgan, T. Sun, D. Holmes, S. Gawad, N.G. Green, Single cell dielectric spectroscopy, J. Phys. D. Appl. Phys. 40 (2007) 6170.
[19] P. Parot, Y.F. Dufrene, P. Hinterdorfer, C. Grimellec, D. Navajas, J.L. Pellequer, S. Scheuring, Past, present and future of atomic force microscopy in life sciences and medicine, J. Mol. Recognit. 20 (2007) 418–431.
[20] W.W. Wilson, M.M. Wade, S.C. Holman, F.R. Champlin, Status of methods for assessing bacterial cell surface charge properties based of zeta potential, J. Microbiol. Meth. 42 (2001) 153–164.
[21] A. Richter-Dahlfors, A.M.J. Buchan, B.B. Finlay, Murine salmonellosis studied by confocal microscopy: *Salmonella typhimurium* resides intracellularly inside macrophages and exerts a cytotoxic effect on phagocytes in vivo, J. Exp. Med. 186 (1997) 569–580.
[22] M. Hope, R. Nayar, L.D. Mayer, P. Cullis, Reduction of liposomes size and preparation of unilamellar vesicles by extrusion techniques, in: G. Gregoriadis (Ed.), Liposome Technology, 2nd edition, volume 1, CRC Press, Boca Raton, FL, 1992, pp. 123–139.
[23] R. MacDonald, R. MacDonald, Applications of freezing and thawing in liposomes technology, in: G. Gregoriadis (Ed.), Liposome Technology, 2nd edition, volume 1, CRC Press, Boca Raton, FL, 1992, pp. 209–228.
[24] V. Berardi, C. Aiello, A. Bonincontro, G. Risuleo, Alterations of the plasma membrane caused by murine polyomavirus proliferation: an electrorotation study, J. Membr. Biol. 229 (2009) 19–25.
[25] T. Yoshimori, A. Yamamoto, Y. Moriyama, M. Futai, Y. Tashiro, Bafilomycin A_1, a specific inhibitor of vacuolar-type H^+-ATPase, inhibits acidification and protein degradation in lysosomes of cultured cells, J. Biol. Chem. 266 (1991) 17707–17712.
[26] U.S. Huth, R. Schubert, R. Peschka-Suss, Investigating the uptake and intracellular fate of pH-sensitive liposomes by flow cytometry and spectral bio-imaging, J. Control Rel. 110 (2006) 490–504.
[27] T. Mosmann, Rapid colorimetric assay for cellular growth and survival: application to proliferation and cytotoxicity assays, J. Immunol. Methods 65 (1983) 55–63.
[28] J. Gimsa, P. Marszalek, U. Loewe, T.Y. Tsong, Dielectrophoresis and elctrorotation of neurospora slime and murine myeloma cells, Biophys. J. 60 (1991) 749–760.
[29] W.M. Arnold, U. Zimmermann, Rotating-field induced rotation and measurement of the membrane capacitance of single mesophyll cells of *Avena sativa*, Z. Naturforsch. C 37 (1982) 908–915.
[30] J. Gimsa, A comprehensive approach to electro-orientation, electrodeformation, dielectrophoresis, and electrorotation of ellipsoidal particles and biological cells, Bioelectrochemistry 54 (2001) 23–31.
[31] U. Kaatze, Dielectric relaxation in aqueous solutions of polyvinylpyrrolidone, Adv. Mol. Relax. Process. 7 (1975) 71–85.
[32] F. Bordi, C. Cametti, R.H. Colby, Dielectric spectroscopy and conductivity of polyelectrolyte solutions, J. Phys. Condens. Matter 16 (2004) R1423–R1463.
[33] F. Bordi, C. Cametti, T. Gili, Reduction of the contribution of electrode polarization effects in the radiowave dielectric measurements of highly conductive biological cell suspensions, Bioelectrochemistry 54 (2001) 53–61.
[34] Q. Zhong, D. Inniss, K. Kjoller, V.B. Elings, Fractured polymer/silica fiber surface studied by tapping mode atomic force microscopy, Surf. Sci. Lett. 290 (1993) L688–L692.
[35] T.A. Camesano, M.J. Natan, B.E. Logan, Observation of changes in bacterial cell morphology using tapping mode atomic force microscopy, Langmuir 16 (2000) 4563–4572.

[36] M.F. Murphy, M.J. Lalor, F.C.R. Manning, F. Lilley, S.R. Crosby, C. Randall, D.V. Burton, Comparative study of the conditions required to image live human epithelial and fibroblast cells using atomic force microscopy, Microsc. Res. Tech. 69 (2006) 757–765.
[37] Q.S. Li, G.Y.H. Lee, C.N. Ong, C.T. Lim, Afm indentation study of breast cancer cells, Biochem. Biophys. Res. Commun. 374 (2008) 609–613.
[38] C.A.J. Putman, K. der Werf, B. Grooth, N. Hulst, J. Greve, Viscoelasticity of living cells allows high resolution imaging by tapping mode atomic force microscopy, Biophys. J. 67 (1994) 1749–1753.
[39] M. Firtel, T. Beveridge, Scanning probe microscopy in microbiology, Micron 26 (1995) 347–362.
[40] Y. Chao, T. Zhang, Optimization of fixation methods for observation of bacterial cell morphology and surface ultrastructures by atomic force microscopy, Appl. Microbiol. Biotechnol. 92 (2011) 381–392.
[41] B. Weyn, W. Kalle, S. Kumar-Singh, E. Marck, H. Tanke, W. Jacob, Atomic force microscopy: influence of air drying and fixation on the morphology and viscoelasticity of cultured cells, J. Microsc. 189 (1998) 172–180.
[42] M. Moloney, L.M. Donnell, H. O'Shea, Atomic force microscopy of BHK-21 cells: an investigation of cell fixation techniques, Ultramicroscopy 100 (2004) 153–161.
[43] W.W. Tscharnuter, Mobility measurements by phase analysis, Appl. Opt. 40 (2001) 3995–4003.
[44] M. Connah, M. Kaszuba, A. Morfesis, High resolution zeta potential measurements: analysis of multi-component mixtures, J. Dispers. Sci. Technol. 23 (2002) 663–669.
[45] M. Minor, A. van der Linde, H. van Leeuwen, J. Lyklema, Dynamic aspects of electrophoresis and electroosmosis: a new fast method for measuring particle mobilities, J. Colloid Interface Sci. 189 (1997) 370–375.
[46] R.J. Hunter, Transport properties of suspensions, in: O. University (Ed.), Foundations of Colloid Science, volume 1, Press, New York, 1993, p. 494563.
[47] D.C.Henry, The cataphoresis of suspended particles. Part I. The equation of cataphoresis, A, Math. Phys. Sci. 133, Proc. Royal. Soc. London, pp. 106–140.
[48] D. Stephens, V. Allan, Light microscopy techniques for live cell imaging, Science 300 (2003) 82–86.
[49] I. Palamá, F. Maria, I. Viola, E. Fabiano, G. Gigli, C. Bettini, G. Barbarella, Live-cell-permeant thiophene fluorophores and cell-mediated formation of fluorescent fibrils, J. Am. Chem. Soc. 133 (2011) 17777–17785.
[50] G.H. Markx, C.L. Davey, The dielectric properties of biological cells at radiofrequencies: applications in biotechnology, Enzym. Microb. Technol. 25 (1999) 161–171.
[51] F. Bordi, C. Cametti, A. Rosi, A. Calcabrini, Frequency domain electrical conductivity measurements of the passive electrical properties of human lymphocytes, Biochim. Biophys. Acta 1153 (1993) 77–88.
[52] J.N. Israelachvili, Intermolecular and Surface Forces, 3rd edition Academic Press - Elsevier, Oxford, UK, 2011.
[53] A. Irimajiri, Y. Doida, T. Hanai, A. Inouye, Passive electrical properties of cultured murine lymphoblast (l5178y) with reference to its cytoplasmic membrane, nuclear envelope, and intracellular phases, J. Membr. Biol. 38 (1978) 209–232.
[54] V. Raicu, C. Gusbeth, D.F. Anghel, G. Turcu, Effects of cetyltrimethylammonium bromide (ctab) surfactant upon the dielectric properties of yeast cells, Biochim. Biophys. Acta 1379 (1998) 7–15.
[55] K. Asami, Dielectric properties of microvillous cells simulated by the three-dimensional finite-element method, Biochemistry 81 (2011) 28–33.
[56] K. Asami, Y. Takahashi, S. Takashima, Dielectric properties of mouse lymphocytes and erythrocytes, Biochim. Biophys. Acta 1010 (1989) 49–55.
[57] X. Hu, W.M. Arnold, U. Zimmermann, Alteration in the electrical properties of T and B lymphocyte membranes induced by mitogenic stimulation. Activation monitored by electro-rotation of single cells, Biochim. Biophys. Acta 1021 (1990) 191–200.
[58] X. Wang, Y. Huang, P.R.C. Gascoyne, F. Becker, R. Holzel, R. Pethig, Changes in friend murine erythroleukaemia cell membranes during induced differentiation determined by electrorotation, Biochim. Biophys. Acta 1193 (1994) 191–200.
[59] S. Aleandri, M.G. Bonicelli, F. Bordi, S. Casciardi, M. Diociaiuti, L. Giansanti, F. Leonelli, G. Mancini, G. Perrone, S. Sennato, How stereochemistry affects the physicochemical features of gemini surfactant based cationic liposomes, Soft Matter 8 (2012) 5904–5915.
[60] D. Ricci, M. Tedesco, M. Grattarola, Mechanical and morphological properties of living 3T6 cells probed via scanning force microscopy, Microsc. Res. Tech. 36 (1997) 165–171.
[61] A. Kusumi, Y. Sako, Cell surface organization by the membrane skeleton, Curr. Opin. Cell Biol. 1768 (1996) 566–574.
[62] J.R. Abney, B.A. Scalettar, Fluctuation and membrane heterogeneity, Biophys. Chem. 57 (1995) 27–36.
[63] T. Dokland, D.W. Hutmacher, M. Mah Lee Ng, J.-T. Schantz, Techniques in microscopy for biomedical applications, volume 2 of manuals in biomed res, World Scientific Pub. Co. Pte. Ltd, Singapore, 2006.
[64] H. Haga, M. Nagayama, K. Kawabata, Imaging mechanical properties of living cells by scanning probe microscopy, Curr. Nanosci. 3 (2007) 97–103.
[65] A.B. Verkhovsky, T.M. Svitkina, G.G. Borisy, Myosin II filament assemblies in the active lamella of fibroblasts: their morphogenesis and role in the formation of actin filament bundles, J. Cell Biol. 131 (1995) 989–1002.
[66] C. Schoenenberger, J.H. Hoh, Slow cellular dynamics in MDCK and R5 cells monitored by time-lapse atomic force microscopy, Biophys. J. 67 (1994) 929–936.
[67] H.X. You, J.M. Lau, S. Zhang, L. Yu, Atomic force microscopy imaging of living cells: a preliminary study of the disruptive effect of the cantilever tip on cell morphology, Ultramicroscopy 82 (2000) 929–936.
[68] J. Domke, W.J. Parak, M. George, H.E. Gaub, M. Radmacher, Mapping the mechanical pulse of single cardiomyocytes with the atomic force microscope, Eur. Biophys. J. 28 (1999) 179–186.
[69] K. Kliche, M. Kuhn, U. Hillebrand, Y. Ludwig, C. Stock, H. Oberleithner, Direct aldosterone action on mouse cardiomyocytes detected with atomic force microscopy, Cell. Physiol. Biochem. 18 (2006) 265–274.
[70] M. Girasole, G. Pompeo, A. Cricenti, A. Congiu-Castellano, F. Andreola, A. Serafino, B. Frazer, G. Boumis, G. Amiconi, Roughness of the plasma membrane as an independent morphological parameter to study RBCs: a quantitative atomic force microscopy investigation, Biochim. Biophys. Acta 1768 (2007) 1268–1276.
[71] M. Girasole, G. Pompeo, A. Cricenti, G. Longo, A. Boumis, G. amd Bellelli, S. Amiconi, The how, when and why of the aging signals appearing on the human erythrocyte membrane: an atomic force microscopy study of surface roughness, Nanomedicine 6 (2010) 760768.
[72] P. D'Antonio, M. Lasalvia, G. Perna, V. Capozzi, Scale-independent roughness value of cell membranes studied by means of afm technique, Biochim. Biophys. Acta 1818 (2012) 3141–3148.
[73] A. Mendez-Vilas, J.M. Bruque, M.L. Gonzalez-Martin, Sensitivity of surface roughness parameters to changes in the density of scanning points in multi-scale AFM studies. Application to a biomaterial surface, Ultramicroscopy 107 (2007) 617–625.
[74] B.N.J. Persson, O. Albohr, U. Tartaglino, A.I. Volokitin, E. Tosatti, On the nature of surface roughness with application to contact mechanics, sealing, rubber friction and adhesion, J. Phys. Condens. Matter 17 (2005) R1–R62.
[75] J.F. Gonzalez Martinez, J. Abad, J. Colchero, Nanoscale measurement of the power spectral density of surface roughness: how to solve a difficult experimental challenge, Nanoscale Res. Lett. 7 (2012) 174–185.
[76] P. Klapetek, D. Necas, C. Anderson, Gwyddion user guide, Czech Metrology Institute, (available on-line at) http://gwyddion.net/documentation/user-guide-en/ 2012.
[77] A.-L. Barabasi, H.E. Stanley, Fractal Concepts in Surface Growth, Cambridge Univ. Press, Cambridge, 1995.
[78] H.A. Abramson, L.S. Moyer, M.H. Gorin, Electrophoresis of Proteins and the Chemistry of Cell Surfaces, Reinhold Publishing Corporation, New York, 1942.
[79] N. Marina-Garcia, L. Franchi, Y. Kim, Y. Hu, D.E. Smith, G.-J. Boons, G. Nunez, Clathrin and dynamin-dependent endocytic pathway regulates muramyl dipeptide internalization and NOD2 activation, J. Immunol. 182 (2009) 4321–4327.
[80] G. Long, X. Pan, R. Kormelink, J.M. Vlak, Functional entry of baculovirus into insect and mammalian cells is dependent on clathrin-mediated endocytosis, J. Virol. 80 (2006) 8830–8833.
[81] Y. Inoue, N. Tanaka, Y. Tanaka, S. Inoue, K. Morita, M. Zhuang, T. Hattori, K. Sugamura, Clathrin-dependent entry of severe acute respiratory syndrome coronavirus into target cells expressing ACE2 with the cytoplasmic tail deleted, J. Virol. 81 (2007) 8722–8729.
[82] E.K. Hoffmann, I.H. Lambert, S.F. Pedersen, Physiology of cell volume regulation in vertebrates, Physiol. Rev. 89 (2009) 193–277.
[83] N. Groulx, F. Boudreault, S.N. Orlov, R. Grygorczyk, Membrane reserves and hypotonic cell swelling, J. Membr. Biol. 214 (2006) 43–56.
[84] S. Aleandri, C. Bombelli, M.G. Bonicelli, F. Bordi, L. Giansanti, G. Mancini, M. Ierino, S. Sennato, Fusion of gemini based cationic liposomes with cell membrane models: implications for their biological activity, Biochim. Biophys. Acta 1828 (2013) 382–390.